Version 30 March 2022

Diffuser: a user-friendly program for diffusion chronometry with robust uncertainty estimation

Li-Guang Wu [1], Yang Li [1] *, Michael C. Jollands [2], Pieter Vermeesch [3], Xian-Hua Li [1]

1, State Key Laboratory of Lithospheric Evolution, Institute of Geology and Geophysics, Chinese Academy of Sciences, Beijing 100029, China

2, Gemological Institute of America, 50 W. 47th St, New York, NY 10036, USA

3, Department of Earth Sciences, University College London, Gower Street, London WC1E 6BT, UK

Submitted to *Computers & Geosciences*

* Corresponding author, Email: geoliy@outlook.com

Abstract

Chemical diffusion in minerals has shown great potential to quantify timescales of geological processes. The presence of chemical gradients, along with favorable temperature and time conditions, lead to the formation of measurable diffusion profiles. Temporal information can be extracted from measured diffusion profiles using either analytical or numerical solutions of Fick's second law. Currently, there is a lack of widely adopted programs for diffusion studies. In addition, the uncertainties associated with timescales derived from diffusion chronometry are critical for geological studies, but are not always robustly evaluated. In many cases, only uncertainties in curve fitting parameters and temperature are considered, whereas other uncertainties, such as those associated with the experimentally determined diffusion coefficients themselves, are rarely propagated into the calculated timescales. Ignoring these uncertainties reduces the reproducibility and intercomparability of results. In response to these challenges, we present Diffuser, a user-friendly program to standardize diffusion chronometry with transparent and robust propagation of uncertainties. Using analytical and numerical methods, our program provides an automatic, visual, and efficient curve fit to extract chronological information from diffusion profiles. The method is complemented by an algorithm to propagate all uncertainties (i.e., measurement, temperature, curve fitting, and diffusion coefficient) to derived timescales. Three examples are provided to highlight how the program can recover timescales with internal consistency, efficient computing and easy-to-use features. Our freely available and user-friendly program will hopefully increase the accessibility and consistency of diffusion modeling and

thereby to facilitate more high-quality diffusion studies.

Keywords: diffusion modeling, timescale, Ti in quartz, Ca in olivine, Li in zircon

1. Introduction

Time is one of the fundamental parameters of earth and planetary sciences, where age and duration are used to put geological events in chronological order and to quantify rates of geological processes, respectively. An absolute age is generally determined by radiometric dating, and two ages can be used to bracket the duration or timescale. This timescale then is used to quantify the rates of geological processes (e.g., Borg et al., 2017; Li et al., 2017; Schoene et al., 2019, 2021; Sprain et al., 2019; Wang et al., 2021). Radiometric dating is routinely used to determine timescales on the order of a few million years and, less frequently, tens to a few thousand years or shorter (e.g., Burgess et al., 2014; Li et al., 2017; Thines et al., 2021). For rapid geological events with shorter timescales (e.g., hours, days, months, and years), constraining their timescales via radiometric dating is very challenging (or even impossible) and requires ultra-high temporal resolution. Complementary to absolute dating, timescales also can be determined through diffusion modeling in minerals (or other phases) regardless of their absolute ages (i.e., diffusion chronometry; Lasaga, 1983), with the potential for diffusion modeling being a function of temperature and time for a given element in a given mineral (Chakraborty, 2008; Costa et al., 2020; Watson and Baxter, 2007; Zhang and Cherniak, 2010). The diffusivity of different elements in minerals varies significantly, hence diffusion chronometry can be used to estimate timescales from a few seconds to several million years (Costa et al., 2020). Whilst diffusion is a thermally activated process and does not require any chemical gradients to operate, the presence of chemical gradients leads to the formation of measurable chemical diffusion profiles.

As soon as a chemical gradient is established, the diffusion clock starts. Element diffusivity depends strongly on temperature, though other factors such as pressure, crystallographic orientation, the fugacities of water and oxygen, and major element activities are important in certain cases (e.g., Ganguly, 2002; Jollands et al., 2016; Kohn and Penniston-Dorland, 2017). The power of diffusion chronometry can be significantly increased by combining multiple elements that simultaneously diffuse with variable diffusivities in a given mineral or in several minerals within the same rock. These can be integrated to provide a more comprehensive understanding of processes that the rock has experienced (Costa et al., 2020; Dohmen et al., 2017).

At the temperature–time conditions relevant to magmatic, metamorphic, and hydrothermal processes, most diffusion in minerals occurs over small length scales (nm to mm). Analytical techniques with high spatial resolution are therefore required to measure changes in composition along the diffusion profiles. In the past few decades, developments in microanalysis techniques such as Fourier-transform infrared spectroscopy, scanning electron microscope, electron microprobe, laser-ablation inductively coupled plasma mass spectrometry, secondary ion mass spectrometry, and local electrode atom probe tomography have accelerated the availability of high-quality diffusion profiles (e.g., Audétat et al., 2021; Bloch et al., 2019; Rubatto et al., 2020; Tang et al., 2017), which have provided critical information to better quantify the timescales of magma storage, ascent, and eruption as well as ore formation, and evolution of metamorphic rocks (e.g., Chu et al., 2018; Cooper, 2019; Devoir et al., 2021; Li et al., 2022; Mutch et al., 2019).

For diffusion studies, Fick's second law lays the foundation for diffusion modeling. Both numerical solutions (e.g., finite difference) and analytical solutions (e.g., Crank, 1975) can be used to solve Fick's second law for the purposes of diffusion chronometry, but a lack of widely accepted protocols for diffusion modeling limits the consistency of different diffusion studies. Hence, a user-friendly program is extremely useful to standardize the usage of diffusion modeling, facilitate more diffusion studies, and enable us to better understand the duration, rate, and efficiency of geological events.

In addition to timescale estimates, diffusion chronometry requires robust propagation of uncertainties. The systematic uncertainties of experimentally determined diffusion coefficients can significantly affect the timescale uncertainties but are rarely considered in current diffusion studies. This impedes objective comparison of timescales derived from different elements. Another problem is that the algorithm of parameter uncertainties in the diffusion coefficients ~~are~~is rarely described in experimental studies, which introduces known but unquantified uncertainties. Available programs for diffusion modeling (e.g., Costa et al., 2008; Dunai, 2005; Faryad and Ježek, 2019; Girona and Costa, 2013; Jollands, 2020; Mutch et al., 2021; Robl et al., 2007; Smye et al., 2018) do not always estimate the aforementioned uncertainties. Therefore, a program that uses an explicit curve-fitting method to determine parameters in the diffusion coefficient and propagates their uncertainties into timescales will make diffusion studies more internally consistent and reproducible.

While all diffusion happens in three-dimensional space, diffusion problems can often be simplified into one-dimensional models, as long as the extent of diffusion is

short relative to the size of the crystal. For demonstration purposes, our program uses analytical solutions to solve the one-dimensional model of single-element diffusion with uncertainties being propagated using the Monte Carlo method. Our program can also be adopted for 2D and 3D scenarios and multi-component systems (i.e., coupled diffusion), which will be available in its future versions.

2. Methodology

Basic notations used in this study are defined in Table 1.

Table 1. Notations used in this study.

Notation	Unit	Description
x	m	position along a diffusion profile
C	as measured	composition along a diffusion profile
C_1, C_2, C_3	as measured	initial compositions of a diffusion profile as defined in Figure 1
erf, erfc		error function (erf) and complementary error function (erfc) used in analytical solutions of a diffusion profile (erfc = 1–erf)
T	K	initial temperature
t	s	diffusion time
D_0	m^2/s	pre-exponential factor in the Arrhenius equation
E_a	J/mol	activation energy in the Arrhenius equation
R	J/(mol·K)	universal gas constant
D	m^2/s	diffusion coefficient

2.1 Analytical solutions to one-dimensional diffusion

The goal of a diffusion problem in one dimension is to solve Fick's second law:

$$\frac{\partial C}{\partial t} = \frac{\partial}{\partial x}\left(D\frac{\partial C}{\partial x}\right) \quad (1)$$

Ideally, this equation can be simplified as follows when D is independent of x and C (equation 2.2 in Crank, 1975):

$$\frac{\partial C}{\partial t} = D\frac{\partial^2 C}{\partial x^2} \quad (2)$$

Analytical solutions to the above equation for diffusion in semi-infinite and infinite media are presented by Crank (1975) and adopted directly in Diffuser. For diffusion in minerals, a semi-infinite medium can be defined as a crystal in contact with an infinite long reservoir of a fixed composition while an infinite medium can be treated as chemical zoning in the interior of a crystal. For instance, in a homogeneous crystal where the boundary is at $x = x_0$ with an initial condition of $x = x_0$, $C = C_1$ at the rim and $x > x_0$, $C = C_2$ in the core (Figure 1A), if diffusion has not appreciably modified the initial core composition, the diffusion profile can be expressed as:

$$C = (C_2 - C_1) \times \mathrm{erf}\left(\frac{x - x_0}{L}\right) + C_1 \quad (3)$$

where L is the characteristic diffusion length and defined as $\sqrt{4Dt}$ when D is independent of time.

It should be emphasized that equation 3 is no longer strictly applicable if diffusion has erased the original core composition. This rule works for the profiles A–F in Figure 1 of a semi-infinite medium. Other analytical solutions to diffusion profiles A–L in Figure 1 can be found in Crank (1975) and the Appendix. While analytical solutions for diffusion profiles A–H in Figure 1 have been compiled in a previous program (PACE), which focuses on deconvoluting the analytical beam effects (Jollands, 2020), Diffuser offers analytical solutions to four more forms of diffusion profiles (I–L in Figure 1) and associated uncertainty estimation of the D or t value. To make Diffuser more versatile, the main functions of PACE (Jollands, 2020) have been incorporated into our program.

2.2 Fitting a model to the diffusion profile

Measured profiles are fitted to the diffusion equations by nonlinear least squares regression (NLS) in MATLAB, which fits functions of the form

$$C = f(x, \beta) + \varepsilon \quad (4)$$

where x and C are observed values, β is the fitted parameter(s), f is the fitted model and ε is the residual error of the model (i.e., the difference between the observed C and the predicted value). NLS finds the model parameter(s) β, which minimizes the residual sum of squares (RSS, equation 5) using an iterative optimization technique (e.g., Levenberg-Marquardt algorithm used in this study; Seber and Wild, 2003). If the uncertainties of C are given (σ), the associated weight of each point also can be considered as $\frac{1}{\sigma^2}$:

$$\mathrm{RSS} = \sum_1^n \frac{1}{\sigma_i^2}(C_i - f(x_i, \beta))^2 \quad (5)$$

where the subscript i denotes the i^{th} value and n is the total number of i.

For profiles A–L (Figure 1), it is straightforward to determine C_1, C_2 and C_3 if a flat compositional platform exists. Although Diffuser can fit a model with C_1, C_2 and C_3 as free parameters, this should not be done in the absence of a flat compositional platform. Specifically, if the flat peak or trough is replaced by a bell shape after diffusion in profiles I–L of Figure 1 (e.g., $t = t_2$), the composition associated with the initial flat peak or trough cannot be determined directly from the composition versus distance data. In such cases, instead of choosing an arbitrary value, Diffuser lets the initial composition vary during modeling, and then also considers its effect on the final timescales. Taking the profile I at $t = t_2$ (Figure 1) as an example, because diffusion

decreases the height and broadens the peak simultaneously, assuming a higher initial composition plateau would result in a narrower initial bandwidth (Figure 2A). As expected, an optimal time value can always be obtained at an assumed flat peak value C_0 (Figure 2B). This means that there exist infinite solutions for the time when a flat compositional plateau is not recognizable for the profile I. Nevertheless, the modeled diffusion time converges with increasing C_0 (Figure 2B), so it is still possible to obtain a time estimate according to a reasonable C_0 or bandwidth, especially if ranges of C_0 can be estimated independently. Taking a diffusion profile of Rubin et al. (2017) as an example, despite C_0 changing considerably, the goodness of fit (R^2) of curve fitting (Figure 2B) shows a very weak response to the choice of C_0. As such, the true initial composition is unknown and using an assumed value will introduce additional uncertainties. Using variable C_0, the maximum timescale is nearly constant (~47 years) when $C_0 > 300$ ppbw (Figure 2B; see the example section for details). To fully account for uncertainties introduced by an unknown initial composition, variable initial compositions are modeled in Diffuser. The same method is applicable to profiles J–L in Figure 1, when a flat compositional peak or trough cannot be recognized.

For profiles K–L in Figure 1, it is noticed that when C_3 is close to the flat peak (or trough) composition, the diffusion profile will resemble Figure 1G–H after sufficient time of diffusion (e.g., t_3 in Figure 1K–L). It should be emphasized that care should be taken to distinguish these two cases in real studies. For instance, profiles of an element with a very low diffusion rate could potentially be used to identify the initial boundary shape.

197

198 **2.3 Time-dependent diffusion coefficient**

199 All the above models apply the parameter L for curve fitting, which equals $\sqrt{4Dt}$

200 when D is independent of time. Here, we consider the case of a non-constant D over

201 time, if, for example, temperature (τ) changes with time (t), then

202 $$\tau(t) = F(T,t) \quad (6)$$

203 where T denotes the initial temperature which is a constant estimated independently

204 by other methods, e.g., geothermometers, and F represents a linear, exponential, or

205 parabolic function.

206 Then, Diffuser employs an isobaric Arrhenius equation for the diffusion coefficient:

207 $$D(t) = D_0 e^{\frac{-E_a}{R\tau(t)}} \quad (7)$$

208 where D_0 and E_a are determined experimentally.

209 Therefore, Dt becomes an integral (ξ):

210 $$\xi(t) = \int_0^t D(t)dt \quad (8)$$

211 and Fick's second law for equation 2 becomes

212 $$\frac{\partial C}{\partial \xi} = \frac{\partial^2 C}{\partial x^2} \quad (9)$$

213 Equation 9 can be solved analytically by replacing Dt with ξ (Crank, 1975). Models

214 can then be fit to data to obtain L and ξ values as:

215 $$L = \sqrt{4\xi} \quad (10)$$

216 The t value can be obtained by solving integral equation 8 directly in MATLAB

217 (e.g., using the fzero function, a combination of bisection, secant, and inverse quadratic

218 interpolation methods). Furthermore, Diffuser outputs the parameter ξ for users to

explore further in case of a more complex time-dependent diffusion coefficient (e.g., an abrupt temperature change caused by magma recharge).

2.4 Uncertainties of the modeled diffusion time

According to previous studies, the uncertainty budget of the modeled diffusion time is dominated by the temperature and parameters that control the diffusion coefficient (Costa et al., 2008; Costa and Morgan, 2010). Diffuser propagates the uncertainties of 1) the parameter L calculated by curve fitting, 2) the initial temperature T estimated by other methods such as geothermometers, 3) and, importantly, the experimentally determined diffusion parameters (D_0 and E_a) themselves, into the uncertainty of the diffusion time. In the case of isothermal diffusion, the relative time uncertainty can be calculated directly as follows, assuming that there is negligible or no covariance between D and L.

$$\left(\frac{\sigma_t}{t}\right)^2 = \left(\frac{\sigma_D}{D}\right)^2 + \left(\frac{2\sigma_L}{L}\right)^2 \quad (11)$$

where σ_t, σ_D and σ_L represent absolute uncertainties of t, D, and L respectively. σ_D is calculated as:

$$\sigma_D = \sqrt{J'\sum J} \quad (12)$$

where $\sum$ is the covariance matrix, J is the Jacobian matrix and J' is its transpose:

$$\sum = \begin{bmatrix} (\sigma_{\ln[D_0]})^2 & \mathrm{Cov}(\ln[D_0], E_a) & 0 \\ \mathrm{Cov}(\ln[D_0], E_a) & (\sigma_{E_a})^2 & 0 \\ 0 & 0 & (\sigma_T)^2 \end{bmatrix} \quad (13)$$

$$J = D\begin{bmatrix} 1 \\ -\frac{1}{RT} \\ \frac{E_a}{RT^2} \end{bmatrix} \quad (14)$$

where $\sigma_{\ln[D_0]}$, σ_{E_a} and σ_T represent absolute uncertainties of ln[D_0], E_a, and T respectively. Cov(ln[D_0],E_a) is the covariance between ln[D_0] and E_a. $\sigma_{\ln[D_0]}$, σ_{E_a} and Cov(ln[D_0],E_a) are calculated in Diffuser by refitting the original experimental data (D at different T) by linear least-squares regression (e.g., Montgomery and Runger, 2018).

If the temperature varies with time (e.g., during cooling), a Monte Carlo method is introduced to estimate the time uncertainty. First, a data set is generated consisting of L_i and T_i values, which follows a Gaussian distribution with uncertainties of σ_L and σ_T, respectively. Second, the diffusion time t_i is calculated using equations 6–10 for each paired L_i and T_i. Finally, we calculate the average t value and its uncertainty from all t_i results. Because t_i values are log-normally distributed based on the Lilliefors test (Figure 3; Lilliefors, 1967), we calculate the average ln[t] value and its uncertainty and then convert them into t, yielding a geometric mean value with upper and lower boundaries at a 95% confidence level. The numerical stability of the geometric mean and confidence interval increases with the number of iterations. Taking a diffusion profile of Rubin et al. (2017) as an example, repeating Monte Carlo modeling 15 times using 100, 500, 1000, 2000, 3000, 4000, and 5000 trials, respectively, shows a convergence of t and its uncertainty (range <1 year) when the number of trials is larger than 2000 (Supplementary Figure S1). In some cases, the distribution of ln[t] values does not follow a normal distribution, and more trials are needed to obtain robust uncertainty estimates.

3. Program design

Diffuser was written in MATLAB and comes with an intuitive graphical user interface (GUI) that can either be used offline (on Windows, Mac or Linux), or online (in any HTML-5 compatible web browser) at http://www.geoapp.cn. The latter is our suggested method for accessing the program regardless of the computer platform being used. A brief introduction of how to use this program interactively is given below. A more detailed manual also is provided along with the program.

3.1 Data input

The measured diffusion profile can be fed into the software through a delimited text (e.g., txt or csv format), spreadsheet file (Microsoft® Excel), or clipboard on the data input panel (Figure 4A). The distance and composition data should be in two columns. If the compositional uncertainties (σ) are assigned in another column, Diffuser asks the user to input the column names of x, C, and σ. Otherwise, all compositional data are treated with equal weights. After data import, the data is directly visualized by means of a pre-formatted plot (Figure 4A).

3.2 Diffusion modeling

After importing the diffusion data, the user can choose the relevant solution to Fick's second law graphically, on the diffusion modeling panel ('Diffusion profile' in Figure 4B) by comparing the shape of the measured data profile with the diffusion types presented in Figure 1. The unit of position x should be set and initial compositions (C_1,

C_2, and C_3) can be fixed or determined by fitting. Specifically, if the user does not define an initial flat peak or trough for profiles I–L in Figure 1, more parameters are required, including minimum and maximum values and a step length of the assumed flat peak or trough (C_0). Then, the user can start a diffusion model to obtain a modeled *Dt* value.

3.3 Time and diffusion coefficient calculation

To model timescales in natural samples, the diffusion coefficient, initial temperature with its uncertainty, trials for the Monte Carlo calculation, and cooling path with its constant coefficient should be set (Figure 4C). Additionally, diffusion coefficient data collected from the literature are provided in an embedded Excel file (see below). The program reads these values automatically and users can access them via a drop-list on the diffusion coefficient panel (Figure 4C) once the program interface is opened. At the time of release, Diffuser contains a library of diffusion coefficients for the following systems: olivine (Ca, Al, P, REE, Ti, H, Li, Be), garnet (Hf, REE), quartz (Ti, Al, H), zircon (REE, Ti, Al, Li), orthopyroxene (REE, Ti, Cr, H), clinopyroxene (Ti, REE, H), and feldspar (Sr, Ba, REE, H). These have been compiled in Diffuser by refitting original experimental data in previous studies. Thus, the algorithm of parameter uncertainties in Diffuser is internally consistent. Diffusion coefficients from other systems can be added ~~into~~to Diffuser by modifying the relevant template file. Requests to add other diffusion coefficients to future versions of Diffuser can be sent to the first author.

To calculate diffusion coefficients in isothermal experimental studies, the user can

enter the experimental duration and get an estimated D with its uncertainty (Figure 4D). Then, the parameters of $\ln[D_0]$ and E_a in the diffusion coefficient and their covariance can be calculated by ordinary linear least-squares regression of experimental data (D at different T).

3.4 Data output

There are two basic types of output in our program after each modeling process: first, a figure showing the curve-fitting result, which can be saved as vector graphics (e.g., Figure 5A); and second, a text or spreadsheet file recording the calculation result (including information of trials, R^2, C_1, C_2, C_3, x_0, Dt, D, t, and t uncertainty). The figure compares the measured diffusion profiles directly with modeled zoning profiles (e.g., Figure 5A). If the temperature is assigned an uncertainty, a marginal plot shows distributions of the temperature and diffusion timescale and the trade-off between these two parameters (e.g, Figure 5B). The uncertainty budget of the diffusion time estimate is broken down into a sequence of histograms that show the contributions of curve fitting, temperature, and experimental parameters in the diffusion coefficient (e.g., Figure 5C).

Especially, during calculation for profiles I–L in Figure 1, if there is no flat peak or trough defined by the user, then an additional figure is created to show the process of estimating timescales with an assumed composition range of the initial flat peak/trough (e.g., Figure 2B). Furthermore, if the temperature decreases with time (non-isothermal systems), Monte Carlo results of timescales are displayed on histograms to show

whether they are log-normally distributed based on the Lilliefors test (e.g., Figure 3). The Monte Carlo results and histograms can be saved so that users can evaluate the calculation process.

4. Examples

We will demonstrate the functionality, convenience and efficiency of Diffuser with three examples.

4.1 Ti diffusion in quartz

Quartz is a common mineral formed in magmatic, metamorphic, and hydrothermal processes. It often has a large crystal size (>>100 μm) and displays clear trace element zoning (e.g., Ti and Al), and thus has been extensively used for diffusion modeling (e.g., Ackerson et al., 2018; Cernuschi et al., 2018; Li et al., 2022; Spear et al., 2012). For example, a titanium diffusion profile in quartz from the Valles caldera, U.S.A. (Boro et al., 2021) yielded a timescale of 180 ± 15 years between magma recharge and volcanic eruption, using the Ti-in-quartz diffusivity of Cherniak et al. (2007) and an assumed temperature of 750 ± 20 °C. Diffuser gives a timescale of 195^{+399}_{-131} years which is identical within uncertainty to the time determined by Boro et al. (2021) using a finite difference method (Figure 5A–B). However, the uncertainty is an order of magnitude larger than that previously estimated. It also can be seen in Diffuser that the main contribution to the time uncertainty is curve fitting (~72%, Figure 5C). In addition, a better way to define the initial diffusion interface position (x_0) is by measuring as many elements as possible and studying transects of slow and fast diffusing elements. In

reality, this is not always possible. Instead of adopting an interface position visually from the diffusion profile, Diffuser determines it directly by curve fitting when an element with a lower diffusivity is unavailable, which is at least convenient and more reproducible.

It should be noted that a recent experimental study of Jollands et al. (2020) yielded a much lower Ti-in-quartz diffusivity than that proposed by Cherniak et al. (2007). Using this new Ti-in-quartz diffusivity will give timescales about three orders of magnitude longer (224^{+1064}_{-185} kyr). This has promoted discussions about addressing the discrepancy of time-scales derived from the two Ti-in-quartz diffusivities (Audétat et al., 2021; Boro et al., 2021; Gualda and Pamukçu, 2020), which is beyond the scope of this study and not discussed further.

4.2 Ca diffusion in olivine

Olivine is a common phenocryst in basalt and has been widely used to constrain timescales between magma intrusion and eruption, which provides important information for volcano monitoring and forecasting. Furthermore, multiple elements including rare earth elements, Ti, P, Cr, Ca, Ni, Fe–Mg, Li, Be, and H in a single olivine crystal enable verifying diffusion and crystal-growth zoning models (see reviews in Costa et al, 2020 and Costa, 2021). Although diffusion of major elements in olivine (e.g., Fe–Mg) shows multi-component effects that generally cannot be modeled using simple analytical solutions of the diffusion equation, trace elements in olivine that have composition-independent diffusivities can be modeled by Diffuser. For example, a Ca

diffusion profile in olivine from the IODP Hole U1309D (Ferrando et al., 2020) records a timescale of 150 ± 40 years for melt-rock interaction, using the Ca-in-olivine diffusivity of Coogan et al. (2005), an initial temperature of 1230 ± 20 °C and linear cooling rate of 0.004 °C/year. Diffuser recovers a timescale of 135^{+86}_{-53} years with a fixed initial CaO composition of 0.065 wt.% at the rim and 0.105 wt.% in the core (Figure 6A–B). This result is identical within uncertainty to the time determined by Ferrando et al. (2020) using a 3D finite difference method. It also can be seen in Diffuser that the main contribution to the time uncertainty is curve fitting (~80%, Figure 6C). Uncertainties of experimentally determined diffusion coefficients are systematic and should be considered when comparing diffusion studies using different elements, or using the same element but different diffusion coefficients.

4.3 Li diffusion in zircon

Zircon is an invaluable mineral for understanding igneous, metamorphic, and sedimentary environments, as highlighted by the wide utilization of its U–Pb ages, trace elements, and Hf–O–Si–Zr isotopes. Trace element diffusion in zircon that recovers magmatic residence time is making it more versatile (e.g., Bloch et al., 2022; Cherniak, 2021; Cherniak and Watson, 2010; Cherniak et al., 2007; Trail et al., 2016). For example, a Li diffusion profile in zircon from the Taupo Volcanic Zone, New Zealand (Rubin et al., 2017) records a timescale of 22 years between magma injection and eruption, using the Li-in-zircon diffusivity of Trail et al. (2016) and a fixed temperature of 700 ± 20 °C. The modeling result of Diffuser (23^{+30}_{-13} years) is identical to the finite difference

method of Rubin et al. (2017) when initial Li compositions are fixed at 0 ppbw outside the band and 120 ppbw in the band (Figure 7A–B). It also can be seen that the major contribution of the time uncertainty comes from the temperature (~60%, Figure 7C). However, because Li diffusion has decreased the initial peak which is now unknown, Rubin et al. (2017) assumed the maximum measured Li composition (~120 ppbw) to represent the initial composition plateau. Such an assumption is plausible but very hard to test. To evaluate the effect of varying initial composition on final timescales, assumed initial Li ~~composition~~compositions ranging from 120 to 600 ppbw are modeled in Diffuser. The results show that obtained timescales range from 23^{+30}_{-13} years to 47^{+60}_{-26} years and have become stable when the maximum Li composition goes beyond ~300 ppbw (Figure 2B). Therefore, it is more reasonable to propagate these uncertainties and use a time range (e.g., 10–107 years) rather than a single value to represent the diffusion time. A more precise time estimate can be obtained if a reasonable plateau value or bandwidth can be constrained. For example, we can consider an upper limit of Li composition in natural zircon for the plateau or use another element with a very low diffusion coefficient (e.g., Hf, Th, and U; Cherniak et al., 1997) to determine the initial bandwidth.

As emphasized by Trail et al. (2016), when Li zoning in zircon is utilized for diffusion chronometry, it is important to evaluate whether Li compositions correlate with the REE and P, which may have charge balance effects related to zircon growth. The potential for such coupled diffusion to modify derived timescales should be evaluated carefully in future diffusion studies.

5. Conclusion

Diffuser is a program designed for diffusion chronometry. In particular, it is coded with robust uncertainty propagation of curve fitting, temperature, and experimentally determined diffusion coefficients. The code offers an intuitive and user-friendly GUI to control the data import, diffusion modeling, time calculation, and diffusivity calculation. The program conducts an automatic curve fit and provides fitting parameters with associated uncertainties. Data output includes figures showing curve-fitting results and text or spreadsheet files recording modeling results which can be saved as vector graphics and used for further processing, respectively. Accelerated by improvements in microanalysis techniques, diffusion profiles at microscales now are readily obtained. Together with the easy-to-handle program to generate diffusion models of multiple elements and multiple minerals, studies on diffusion timescales are expected to become more common for a more comprehensive understanding on the duration and rates of geological processes.

Authorship statement

Y. Li designed the project with inputs from P. Vermeesch, M. Jollands and X.H. Li; L.G. Wu and Y. Li developed the methodology and software, and wrote the initial draft. All authors contributed to the revisions, led by Y. Li.

Declaration of competing interest

The authors declare that they have no known competing financial interests nor personal relationships

that could have appeared to influence the work reported in this paper.

Acknowledgments

This study was supported by the National Natural Science Foundation of China (Grant 42022022 and 42103022), the Experimental Technology Innovation Fund of the Institute of Geology and Geophysics, Chinese Academy of Sciences (Grant TEC202105) and the Pioneer Hundred Talents Program of Chinese Academy of Sciences. This is a contribution to the DDE (Deep-Time Digital Earth) Big Science Program. Y. Li thanks Prof. Jeroen Van-Hunen and the NERC Advanced Training Course for developing his coding skills and learning diffusion modeling. We thank two anonymous reviewers and editor Pierre Lanari for very constructive comments that significantly improved the quality and presentation of this paper and the program.

Computer code availability

The source code and user manual of Diffuser can be downloaded from https://github.com/liguangwu/diffuser.git and a web version of Diffuser is available at http://www.geoapp.cn/. Comments, bug reports, and requests for extra diffusion coefficients to be added to the database can be sent to the authors via wuliguang@mail.iggcas.ac.cn (L.G. Wu) and geoliy@outlook.com (Y. Li).

References

Ackerson, M.R., Mysen, B.O., Tailby, N.D., Watson, E.B., 2018. Low-temperature crystallization of granites and the implications for crustal magmatism. Nature 559, 94-97. https://doi.org/10.1038/s41586-018-0264-2

Audétat, A., Miyajima, N., Wiesner, D., Audinot, J.-N., 2021. Confirmation of slow Ti diffusion in quartz by diffusion couple experiments and evidence from natural samples. Geology 49, 963-967. https://doi.org/10.1130/G48785.1

Bloch, E.M., Jollands, M.C., Gerstl, S.S.A., Bouvier, A.S., Plane, F., Baumgartner, L.P., 2019. Diffusion of calcium in forsterite and ultra-high resolution of experimental diffusion profiles in minerals using local electrode atom probe tomography. Geochimica Et Cosmochimica Acta 265, 85-95. https://doi.org/10.1016/j.gca.2019.09.003

Bloch, E.M., Jollands, M.C., Tollan, P., Plane, F., Bouvier, A.S., Hervig, R., Berry, A.J., Zaubitzer, C., Escrig, S., Müntener, O., Ibañez-Mejia, M., Alleon, J., Meibom, A., Baumgartner, L.P., Marin-Carbonne, J., Newville, M., 2022. Diffusion anisotropy of Ti in zircon and implications for Ti-in-zircon thermometry. Earth and Planetary Science Letters 578, 117317. https://doi.org/10.1016/j.epsl.2021.117317

Borg, L.E., Connelly, J.N., Cassata, W.S., Gaffney, A.M., Bizzarro, M., 2017. Chronologic implications for slow cooling of troctolite 76535 and temporal relationships between the Mg-suite and the

ferroan anorthosite suite. Geochimica Et Cosmochimica Acta 201, 377-391. 10.1016/j.gca.2016.11.021

Boro, J.R., Wolff, J.A., Neill, O.K., Steiner, A.R., Ramos, F.C., 2021. Titanium diffusion profiles and melt inclusion chemistry and morphology in quartz from the Tshirege Member of the Bandelier Tuff. American Mineralogist 106, 620-632. https://doi.org/10.2138/am-2021-7395

Burgess, S.D., Bowring, S., Shen, S.-z., 2014. High-precision timeline for Earth's most severe extinction. Proceedings of the National Academy of Sciences 111, 3316-3321. https://doi.org/10.1073/pnas.1317692111

Cernuschi, F., Dilles, J.H., Grocke, S.B., Valley, J.W., Kitajima, K., Tepley, F.J., III, 2018. Rapid formation of porphyry copper deposits evidenced by diffusion of oxygen and titanium in quartz. Geology 46, 611-614. https://doi.org/10.1130/G40262.1

Chakraborty, S., 2008. Diffusion in solid silicates: A tool to track timescales of processes comes of age. Annual Review of Earth and Planetary Sciences 36, 153-190. https://doi.org/10.1146/annurev.earth.36.031207.124125

Cherniak, D.J., 2021. Aluminum diffusion in zircon. Chemical Geology 584, 120510. https://doi.org/10.1016/j.chemgeo.2021.120510

Cherniak, D.J., Hanchar, J.M., Watson, E.B., 1997. Diffusion of tetravalent cations in zircon. Contributions to Mineralogy and Petrology 127, 383-390. https://doi.org/10.1007/s004100050287

Cherniak, D.J., Watson, E.B., 2010. Li diffusion in zircon. Contributions to Mineralogy and Petrology 160, 383-390. https://doi.org/10.1007/s00410-009-0483-5

Cherniak, D.J., Watson, E.B., Wark, D.A., 2007. Ti diffusion in quartz. Chemical Geology 236, 65-74. https://doi.org/10.1016/j.chemgeo.2006.09.001

Chu, X., Ague, J.J., Tian, M., Baxter, E.F., Rumble, D., III, Chamberlain, C.P., 2018. Testing for rapid thermal pulses in the crust by modeling garnet growth–diffusion–resorption profiles in a UHT metamorphic 'hot spot', New Hampshire, USA. Journal of Petrology 59, 1939-1964. https://doi.org/10.1093/petrology/egy085

Coogan, L.A., Hain, A., Stahl, S., Chakraborty, S., 2005. Experimental determination of the diffusion coefficient for calcium in olivine between 900°C and 1500°C. Geochimica Et Cosmochimica Acta 69, 3683-3694. https://doi.org/10.1016/j.gca.2005.03.002

Cooper, K.M., 2019. Time scales and temperatures of crystal storage in magma reservoirs: implications for magma reservoir dynamics. Philosophical Transactions of the Royal Society A: Mathematical, Physical and Engineering Sciences 377, 20180009. https://doi.org/10.1098/rsta.2018.0009

Costa, F., 2021. Clocks in magmatic rocks. Annual Review of Earth and Planetary Sciences 49, 231-252. https://doi.org/10.1146/annurev-earth-080320-060708

Costa, F., Dohmen, R., Chakraborty, S., 2008. Time scales of magmatic processes from modeling the zoning patterns of crystals. Reviews in mineralogy and geochemistry 69, 545-594. https://doi.org/10.2138/rmg.2008.69.14

Costa, F., Morgan, D., 2010. Time constraints from chemical equilibration in magmatic crystals, In: Dosseto, A., Turner, S.P., Van Orman, J.A. (Eds.), Timescales of Magmatic Processes: From Core to Atmosphere. John Wiley & Sons, Chichester, West Sussex, UK, pp. 125-159.

514 Costa, F., Shea, T., Ubide, T., 2020. Diffusion chronometry and the timescales of magmatic processes.
515 Nature Reviews Earth & Environment 1, 201-214. https://doi.org/10.1038/s43017-020-0038-x

516 Crank, J., 1975. The mathematics of diffusion, 2 edn. Oxford University Press, London.

517 Devoir, A., Bloch, E., Müntener, O., 2021. Residence time of igneous garnet in Si-rich magmatic systems:
518 Insights from diffusion modeling of major and trace elements. Earth and Planetary Science Letters
519 560, 116771. https://doi.org/10.1016/j.epsl.2021.116771

520 Dimanov, A., Wiedenbeck, M., 2006. (Fe,Mn)-Mg interdiffusion in natural diopside: effect of pO2.
521 European Journal of Mineralogy 18, 705-718. https://doi.org/10.1127/0935-1221/2006/0018-0705

522 Dohmen, R., Faak, K., Blundy, J.D., 2017. Chronometry and speedometry of magmatic processes using
523 chemical diffusion in olivine, plagioclase and pyroxenes. Reviews in mineralogy and geochemistry
524 83, 535-575. https://doi.org/10.2138/rmg.2017.83.16

525 Dunai, T.J., 2005. Forward modeling and interpretation of (U-Th)/He ages. Reviews in mineralogy and
526 geochemistry 58, 259-274. https://doi.org/10.2138/rmg.2005.58.10

527 Faryad, S.W., Ježek, J., 2019. Compositional zoning in garnet and its modification by diffusion during
528 pressure and temperature changes in metamorphic rocks; an approach and software. Lithos 332-
529 333, 287-295. https://doi.org/10.1016/j.lithos.2019.03.002

530 Ferrando, C., Lynn, K.J., Basch, V., Ildefonse, B., Godard, M., 2020. Retrieving timescales of oceanic
531 crustal evolution at Oceanic Core Complexes: Insights from diffusion modelling of geochemical
532 profiles in olivine. Lithos 376-377, 105727. https://doi.org/10.1016/j.lithos.2020.105727

533 Ganguly, J., 2002. Diffusion kinetics in minerals: principles and applications to tectono-metamophic
534 processes, In: Gramaccioli, C.M. (Ed.), Energy Modelling in Minerals. Eötvös University Press,
535 Budapest, pp. 271-309.

536 Girona, T., Costa, F., 2013. DIPRA: A user-friendly program to model multi-element diffusion in olivine
537 with applications to timescales of magmatic processes. Geochemistry, Geophysics, Geosystems 14,
538 422-431. https://doi.org/10.1029/2012GC004427

539 Gualda, G.A.R., Pamukçu, A.S., 2020. New Ti-in-quartz diffusivities reconcile natural Ti zoning with
540 time scales and temperatures of upper crustal magma reservoirs: COMMENT. Geology 48, e513-
541 e513. https://doi.org/10.1130/G48242C.1

542 Jollands, M.C., 2020. Assessing analytical convolution effects in diffusion studies: Applications to
543 experimental and natural diffusion profiles. PLOS ONE 15, e0241788.
544 https://doi.org/10.1371/journal.pone.0241788

545 Jollands, M.C., Bloch, E., Müntener, O., 2020. New Ti-in-quartz diffusivities reconcile natural Ti zoning
546 with time scales and temperatures of upper crustal magma reservoirs. Geology 48, 654-657.
547 https://doi.org/10.1130/G47238.1

548 Jollands, M.C., Hermann, J., O'Neill, H.S.C., Spandler, C., Padrón-Navarta, J.A., 2016. Diffusion of Ti
549 and some Divalent Cations in Olivine as a Function of Temperature, Oxygen Fugacity, Chemical
550 Potentials and Crystal Orientation. Journal of Petrology 57, 1983-2010.
551 https://doi.org/10.1093/petrology/egw067

552 Kohn, M.J., Penniston-Dorland, S.C., 2017. Diffusion: Obstacles and opportunities in petrochronology.
553 Reviews in mineralogy and geochemistry 83, 103-152. https://doi.org/10.2138/rmg.2017.83.4

Lasaga, A.C., 1983. Geospeedometry: An Extension of Geothermometry, In: Saxena, S.K. (Ed.), Kinetics and Equilibrium in Mineral Reactions, 1 ed. Springer, New York, NY, pp. 81-114.

Li, Y., Mark, A.B., Li, X.-H., 2022. Millennial pulses of ore formation and an extra-high Tibetan Plateau. Geology. https://www.doi.org/10.1130/G49911.1

Li, Y., Selby, D., Condon, D., Tapster, S., 2017. Cyclic magmatic-hydrothermal evolution in porphyry systems: High-precision U-Pb and Re-Os geochronology constraints on the Tibetan Qulong porphyry Cu-Mo deposit. Economic Geology 112, 1419-1440. https://doi.org/10.5382/econgeo.2017.4515

Lilliefors, H.W., 1967. On the kolmogorov-smirnov test for normality with mean and variance unknown. Journal of the American Statistical Association 62, 399-402. https://doi.org/10.1080/01621459.1967.10482916

Montgomery, D.C., Runger, G.C., 2018. Applied statistics and probability for engineers, 7 edn. John Wiley & Sons, Inc., New York, United States.

Mutch, E.J.F., Maclennan, J., Holland, T.J.B., Buisman, I., 2019. Millennial storage of near-Moho magma. Science 365, 260-264. https://doi.org/10.1126/science.aax4092

Mutch, E.J.F., Maclennan, J., Shorttle, O., Rudge, J.F., Neave, D.A., 2021. DFENS: Diffusion chronometry using finite elements and nested sampling. Geochemistry, Geophysics, Geosystems 22, e2020GC009303. https://doi.org/10.1029/2020GC009303

Robl, J., Hergarten, S., Stüwe, K., Hauzenberger, C., 2007. THERMAL HISTORY: A new software to interpret diffusive zoning profiles in garnet. Computers & Geosciences 33, 760-772. https://doi.org/10.1016/j.cageo.2006.10.010

Rubatto, D., Burger, M., Lanari, P., Hattendorf, B., Schwarz, G., Neff, C., Keresztes Schmidt, P., Hermann, J., Vho, A., Günther, D., 2020. Identification of growth mechanisms in metamorphic garnet by high-resolution trace element mapping with LA-ICP-TOFMS. Contributions to Mineralogy and Petrology 175, 61. https://doi.org/10.1007/s00410-020-01700-5

Rubin, A.E., Cooper, K.M., Till, C.B., Kent, A.J.R., Costa, F., Bose, M., Gravley, D., Deering, C., Cole, J., 2017. Rapid cooling and cold storage in a silicic magma reservoir recorded in individual crystals. Science 356, 1154-1156. https://doi.org/10.1126/science.aam8720

Schoene, B., Eddy, M.P., Keller, C.B., Samperton, K.M., 2021. An evaluation of Deccan Traps eruption rates using geochronologic data. Geochronology 3, 181-198. https://doi.org/10.5194/gchron-3-181-2021

Schoene, B., Eddy, M.P., Samperton, K.M., Keller, C.B., Keller, G., Adatte, T., Khadri, S.F.R., 2019. U-Pb constraints on pulsed eruption of the Deccan Traps across the end-Cretaceous mass extinction. Science 363, 862-866. https://www.doi.org/10.1126/science.aau2422

Seber, G.A., Wild, C.J., 2003. Nonlinear regression. John Wiley & Sons, Inc., Hoboken, New Jersey.

Smye, A.J., Marsh, J.H., Vermeesch, P., Garber, J.M., Stockli, D.F., 2018. Applications and limitations of U-Pb thermochronology to middle and lower crustal thermal histories. Chemical Geology 494, 1-18. https://doi.org/10.1016/j.chemgeo.2018.07.003

Spear, F.S., Ashley, K.T., Webb, L.E., Thomas, J.B., 2012. Ti diffusion in quartz inclusions: implications for metamorphic time scales. Contributions to Mineralogy and Petrology 164, 977-986.

https://doi.org/10.1007/s00410-012-0783-z

Sprain, C.J., Renne, P.R., Vanderkluysen, L., Pande, K., Self, S., Mittal, T., 2019. The eruptive tempo of Deccan volcanism in relation to the Cretaceous-Paleogene boundary. Science 363, 866-870. https://www.doi.org/10.1126/science.aav1446

Tang, M., Rudnick, R.L., McDonough, W.F., Bose, M., Goreva, Y., 2017. Multi-mode Li diffusion in natural zircons: Evidence for diffusion in the presence of step-function concentration boundaries. Earth and Planetary Science Letters 474, 110-119. https://doi.org/10.1016/j.epsl.2017.06.034

Thines, J.E., Ukstins, I.A., Wall, C., Schmitz, M., 2021. Volumetric extrusive rates of silicic supereruptions from the Afro-Arabian large igneous province. Nature Communications 12, 6299. https://doi.org/10.1038/s41467-021-26468-5

Trail, D., Cherniak, D.J., Watson, E.B., Harrison, T.M., Weiss, B.P., Szumila, I., 2016. Li zoning in zircon as a potential geospeedometer and peak temperature indicator. Contributions to Mineralogy and Petrology 171, 25. https://doi.org/10.1007/s00410-016-1238-8

Wang, J.-M., Lanari, P., Wu, F.-Y., Zhang, J.-J., Khanal, G.P., Yang, L., 2021. First evidence of eclogites overprinted by ultrahigh temperature metamorphism in Everest East, Himalaya: Implications for collisional tectonics on early Earth. Earth and Planetary Science Letters 558, 116760. https://doi.org/10.1016/j.epsl.2021.116760

Watson, E.B., Baxter, E.F., 2007. Diffusion in solid-Earth systems. Earth and Planetary Science Letters 253, 307-327. https://doi.org/10.1016/j.epsl.2006.11.015

Zhang, Y., Cherniak, D.J., 2010. Diffusion in minerals and melts, 1 edn. Reviews in Mineralogy and Geochemistry, Boston.

List of Figures

Figure 1. **A–D**, half diffusion profiles from rim to core in a crystal; **E–F**, full diffusion profiles from rim to rim in a crystal. **G–H**, diffusion profiles for chemical zoning with an initial sharp boundary in a crystal; **I–L**, diffusion profiles for chemical zoning with an initially confined band in a crystal. The grey dashed line shows the initial boundary and composition conditions at time t_0 ($t_0 = 0$) and the blue solid line shows the diffusion profile at time t_1, t_2, and t_3 ($t_0<t_1<t_2<t_3$). The right panel shows composition distributions within minerals before ($t = t_0$) and after diffusion ($t = t_1$) which corresponds to profiles A–L, respectively. The black arrow shows the direction of the diffusive flux.

Figure 2. **A**, a schematic diagram showing that different values of the initial flat peak and bandwidth can have a same diffusion profile. **B**, modeled diffusion time with an assumed composition range of the initial flat peak using an example data from Rubin et al. (2017). Uncertainties of the curve fitting, temperature and experimentally determined diffusion coefficient are propagated into the uncertainty of timescales.

Figure 3. Distribution of ln[t] and timescales calculated by the Monte Carlo method (with an artificial cooling rate of 200 °C/Ma and temperature of 700 ± 20 °C) using an example data from Rubin et al. (2017). Trials are 5000 in total.

Figure 4. A screenshot of Diffuser interface. **A**, data import panel. **B**, diffusion modeling panel. **C**, time calculation panel. **D**, diffusivity calculation panel.

637

638 **Figure 5**. An example of Ti-in-quartz diffusion modeling in Diffuser using raw data
639 from Boro et al. (2021). **A**, curve fitting result of the diffusion profile. **B**, marginal plot
640 showing distributions of the temperature and diffusion timescale and the trade-off
641 between these two parameters. The superscript a and b denote timescales calculated by
642 the finite difference method from Boro et al. (2021) and by Diffuser, respectively. **C**,
643 histogram showing the uncertainty budget of modeled timescales.

644

645 **Figure 6**. An example of Ca-in-olivine diffusion modeling in Diffuser using raw data
646 from Ferrando et al. (2020). **A**, curve fitting result of the diffusion profile. **B**, marginal
647 plot showing distributions of the temperature and diffusion timescale and the trade-off
648 between these two parameters. The superscript a and b denote timescales calculated by
649 the finite difference method from Ferrando et al. (2020) and by Diffuser, respectively.
650 **C**, histogram showing the uncertainty budget of the modeled timescale.

651

652 **Figure 7**. An example of Li-in-zircon diffusion modeling in Diffuser using raw data
653 from Rubin et al. (2017). A, curve fitting result of the diffusion profile. B, marginal plot
654 showing distributions of the temperature and diffusion timescale and the trade-off
655 between these two parameters. The superscript a and b denote timescales calculated by
656 the finite difference method from Rubin et al. (2017) and by Diffuser, respectively. C,
657 histogram showing the uncertainty budget of the modeled timescale.

658
659

Appendix

Analytical solutions to diffusion in semi-infinite and infinite media are listed below.

1 Diffusion in a semi-infinite medium

For a rim-to-core profile with an initial condition of $x = x_0$, $C = C_1$ and $x > x_0$, $C = C_2$ (Figure 1A):

$$C = (C_2 - C_1) \times \mathrm{erf}\left(\frac{x - x_0}{L}\right) + C_1 \quad \text{(A1)}$$

For a rim-to-core profile with an initial condition of $x < x_0$, $C = C_2$ and $x = x_0$, $C = C_1$ (Figure 1B):

$$C = (C_2 - C_1) \times \mathrm{erf}\left(\frac{-x + x_0}{L}\right) + C_1 \quad \text{(A2)}$$

For a rim-to-core profile with an initial condition of $x = x_0$, $C = C_2$ and $x > x_0$, $C = C_1$ (Figure 1C; analogous to equation 2.45 in Crank, 1975):

$$C = (C_2 - C_1) \times \mathrm{erfc}\left(\frac{x - x_0}{L}\right) + C_1 \quad \text{(A3)}$$

For a rim-to-core profile with an initial condition of $x < x_0$, $C = C_1$ and $x = x_0$, $C = C_2$ (Figure 1D):

$$C = (C_2 - C_1) \times \mathrm{erfc}\left(\frac{-x + x_0}{L}\right) + C_1 \quad \text{(A4)}$$

For a rim-to-rim profile with an initial condition of $(x_0 - W) < x < (x_0 + W)$, $C = C_2$ and $x \leqslant (x_0 - W)$ or $x \geqslant (x_0 + W)$, $C = C_1$ (Figure 1E):

$$C = (C_2 - C_1) \times \left[\mathrm{erf}\left(\frac{W + x - x_0}{L}\right) + \mathrm{erf}\left(\frac{W - x + x_0}{L}\right)\right] + 2C_1 - C_2 \quad \text{(A5)}$$

where W is the rim-to-core length.

For a rim-to-rim profile with an initial condition of $(x_0 - W) < x < (x_0 + W)$, $C = C_1$ and $x \leqslant (x_0 - W)$ or $x \geqslant (x_0 + W)$, $C = C_2$ (Figure 1F):

$$C = (C_2 - C_1) \times \left[\operatorname{erfc}\left(\frac{W+x-x_0}{L}\right) + \operatorname{erfc}\left(\frac{W-x+x_0}{L}\right)\right] + C_1 \quad \text{(A6)}$$

2 Diffusion in an infinite medium

For an initial sharp boundary when the position of the initial diffusion interface is fixed at $x = x_0$ (Figure 1G), if an initial high composition (C_2) lies on the right side,

$$C = \frac{C_2 - C_1}{2} \times \left[1 + \operatorname{erf}\left(\frac{x-x_0}{L}\right)\right] + C_1 \quad \text{(A7)}$$

If an initial high composition (C_2) lies on the left side (Figure 1H; analogous to equation 2.14 in Crank, 1975),

$$C = \frac{C_2 - C_1}{2} \times \operatorname{erfc}\left(\frac{x-x_0}{L}\right) + C_1 \quad \text{(A8)}$$

For an initially confined region of $(x_0-h)<x<(x_0+h)$, if the diffusion is symmetric with an initial high composition (C_2) in the region (Figure 1I; analogous to equation 2.15 in Crank, 1975),

$$C = \frac{C_2 - C_1}{2} \times \left[\operatorname{erf}\left(\frac{h-x+x_0}{L}\right) + \operatorname{erf}\left(\frac{h+x-x_0}{L}\right)\right] + C_1 \quad \text{(A9)}$$

where h is the half bandwidth.

If the diffusion profile is symmetric with an initial low composition (C_1) in the region (Figure 1J),

$$C = \frac{C_2 - C_1}{2} \times \left[\operatorname{erfc}\left(\frac{h-x+x_0}{L}\right) + \operatorname{erfc}\left(\frac{h+x-x_0}{L}\right)\right] + C_1 \quad \text{(A10)}$$

If the diffusion profile is asymmetric with an initial high composition (C_2) in the region (Figure 1K),

$$C = \frac{C_2 - C_3}{2} \times \operatorname{erf}\left(\frac{h-x+x_0}{L}\right) + \frac{C_2 - C_1}{2} \times \operatorname{erf}\left(\frac{h+x-x_0}{L}\right) + \frac{C_3}{2} + \frac{C_1}{2} \quad \text{(A11)}$$

If the diffusion profile is asymmetric with an initial low composition (C_1) in the region (Figure 1L),

$$C = \frac{C_3 - C_1}{2} \times \mathrm{erfc}\left(\frac{h - x + x_0}{L}\right) + \frac{C_2 - C_1}{2} \times \mathrm{erfc}\left(\frac{h + x - x_0}{L}\right) + C_1 \quad \text{(A12)}$$

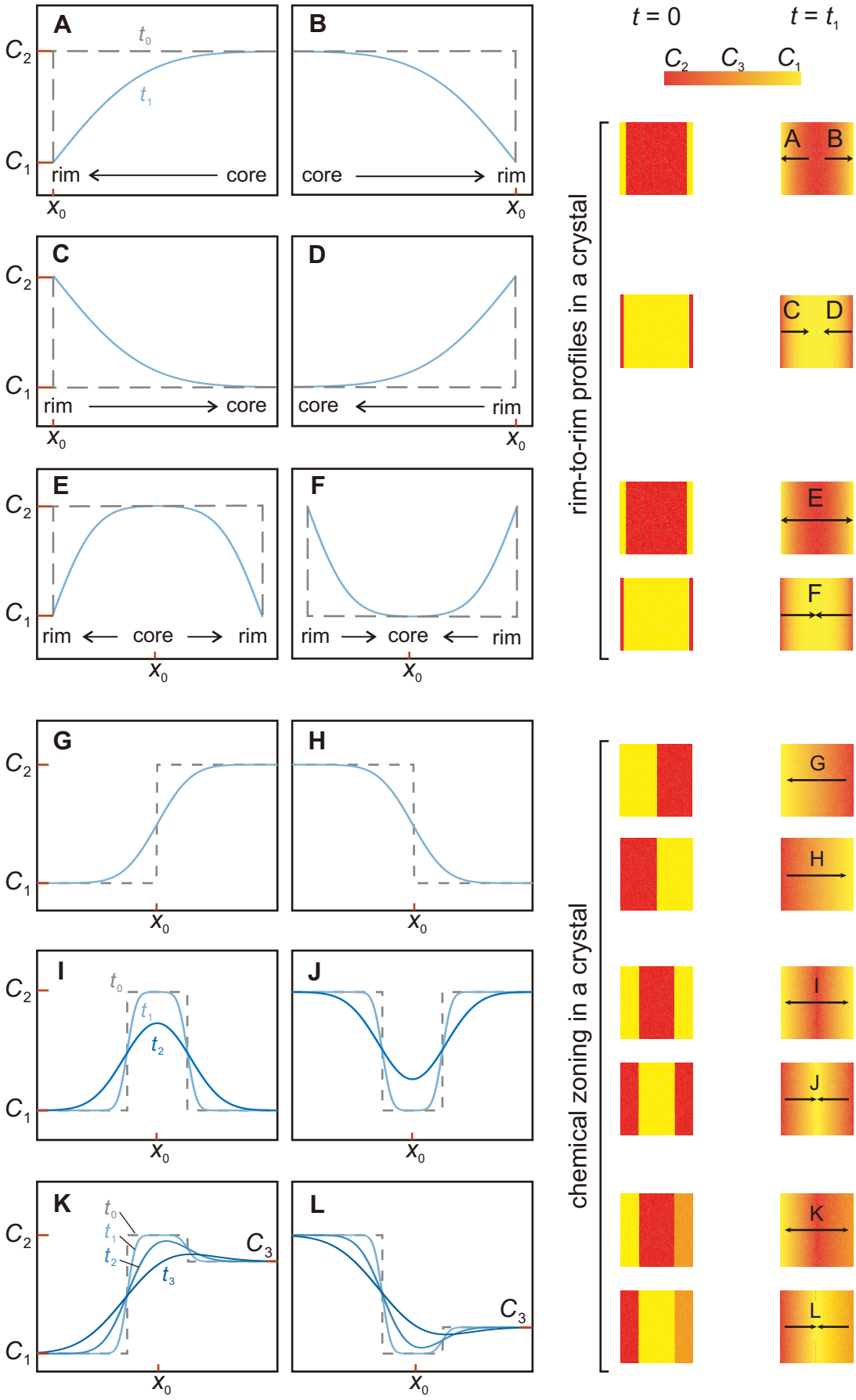
A
B
C
D
E
F
G
H
I
J
K
L
C_2
C_1
C_3
t_0
t_1
t_2
t_3
x_0
rim
core
$t = 0$
$t = t_1$
rim-to-rim profiles in a crystal
chemical zoning in a crystal

Figure 1

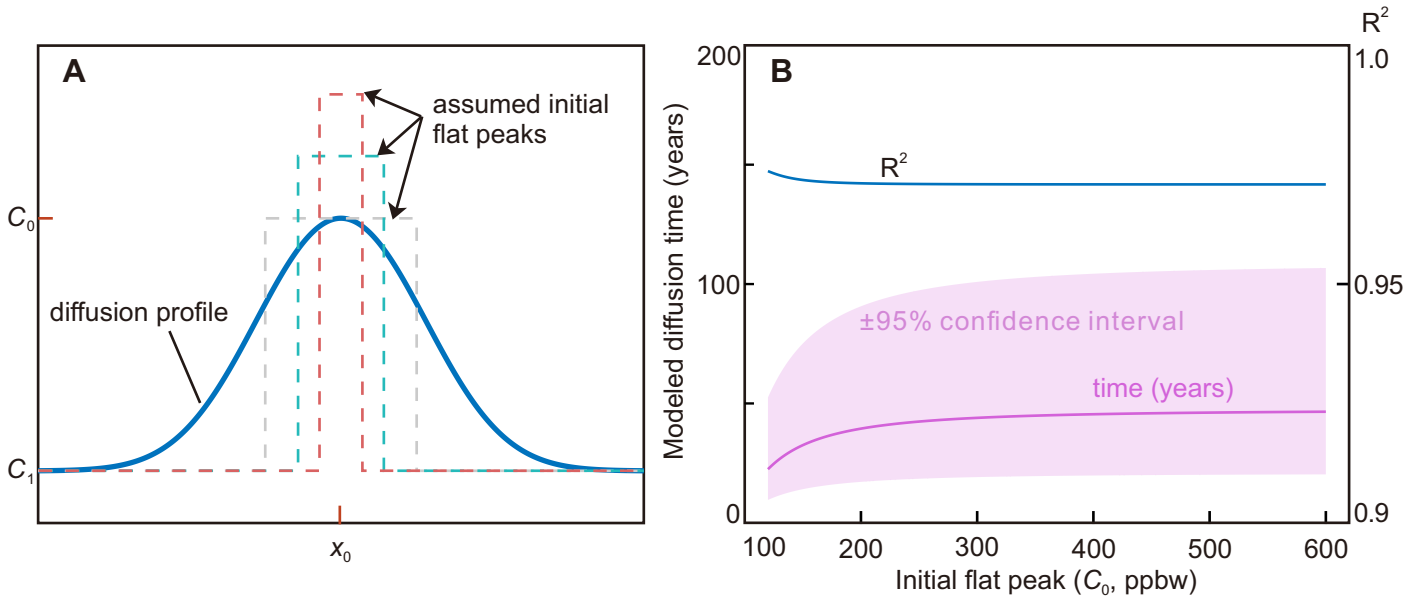
A
assumed initial
flat peaks
C_0
diffusion profile
C_1
x_0
B
R^2
200
100
0
1.0
0.95
0.9
Modeled diffusion time (years)
R^2
±95% confidence interval
time (years)
100
200
300
400
500
600
Initial flat peak (C_0, ppbw)

Figure 2

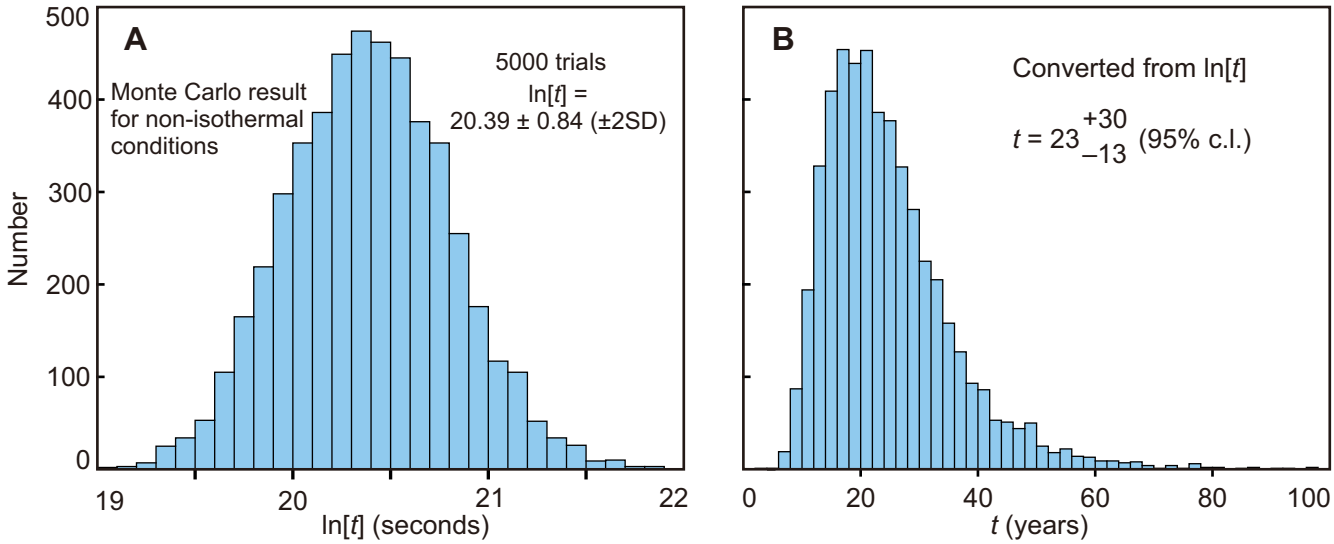
A
Monte Carlo result
for non-isothermal
conditions
5000 trials
ln[t] =
20.39 ± 0.84 (±2SD)
Number
500
400
300
200
100
0
19
20
21
22
ln[t] (seconds)
B
Converted from ln[t]
t = 23 +30 −13 (95% c.l.)
0
20
40
60
80
100
t (years)

Figure 3

A. data import

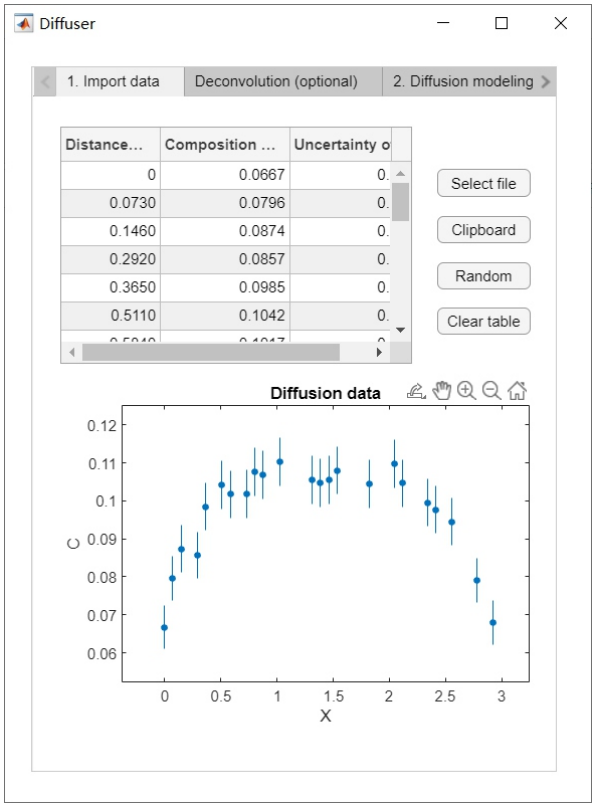

B. diffusion modeling

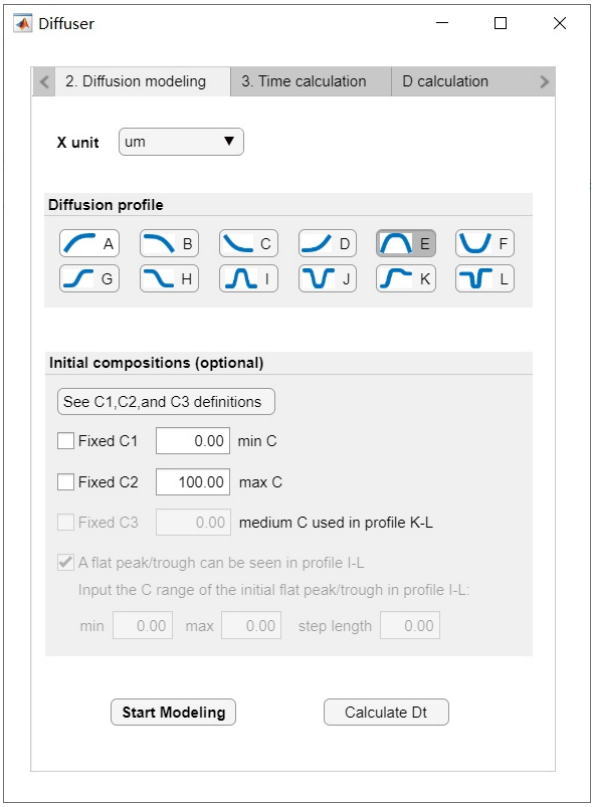

C. time calculation

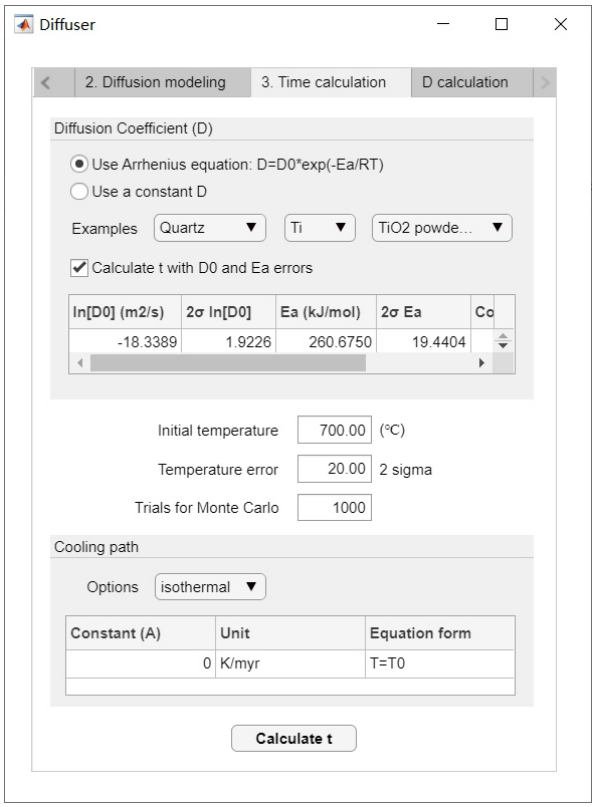

D. diffusivity calculation

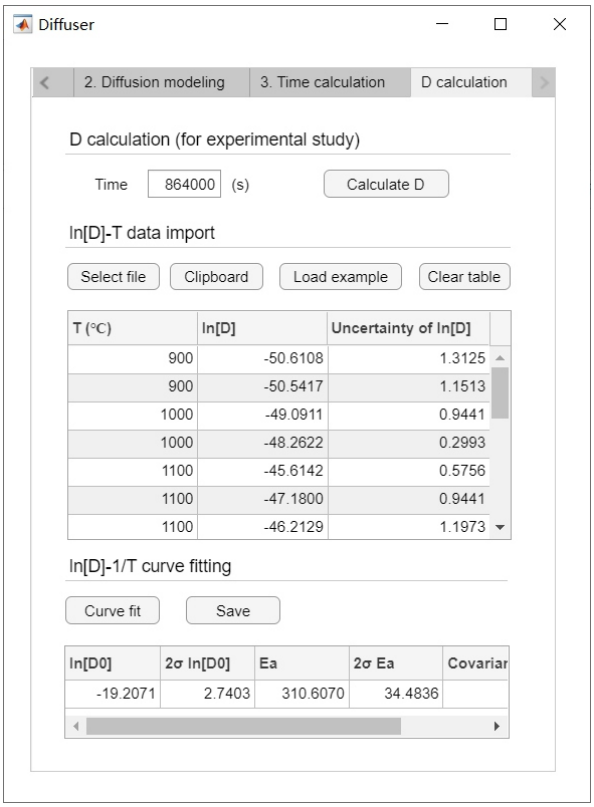

Figure 4

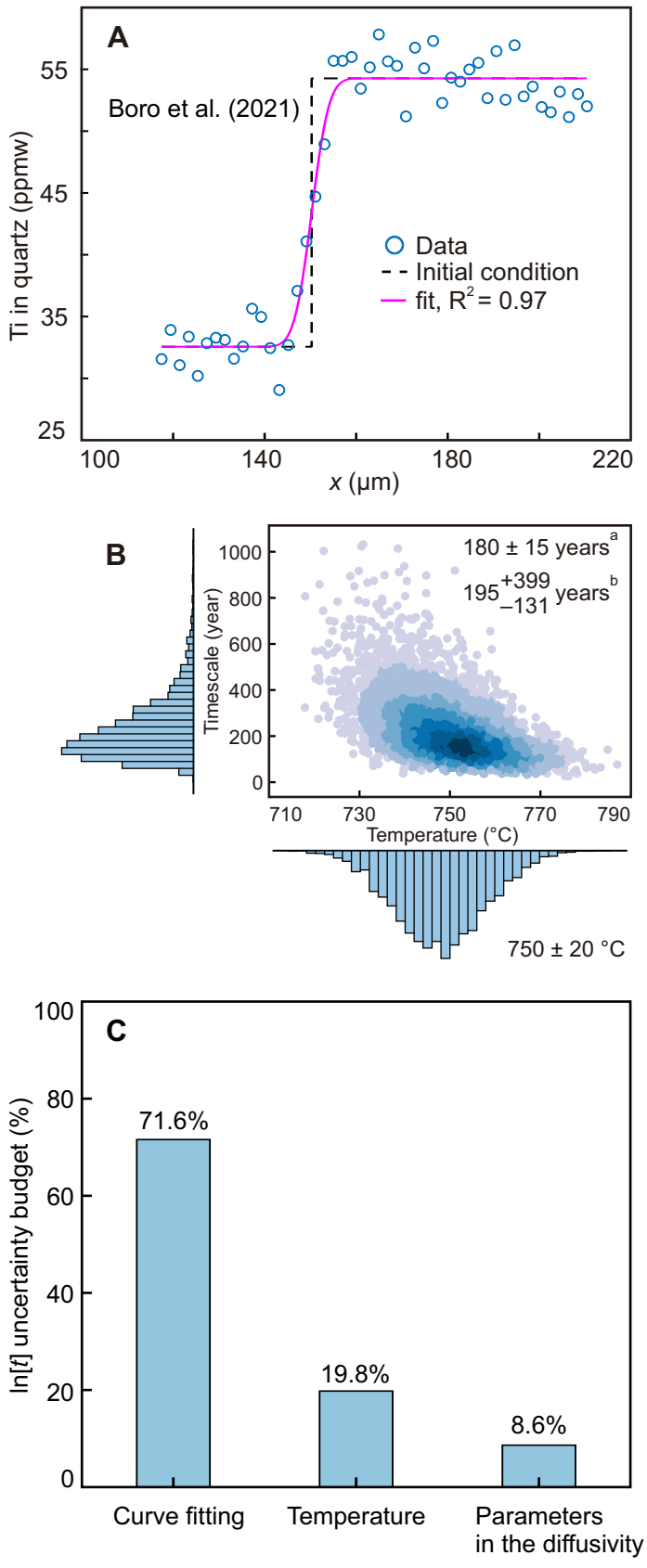
A
Boro et al. (2021)
Ti in quartz (ppmw)
55
45
35
25
100
140
180
220
x (μm)
Data
Initial condition
fit, R² = 0.97
B
180 ± 15 years[a]
195 +399 −131 years[b]
Timescale (year)
1000
800
600
400
200
0
710
730
750
770
790
Temperature (°C)
750 ± 20 °C
C
ln[t] uncertainty budget (%)
100
80
60
40
20
0
71.6%
19.8%
8.6%
Curve fitting
Temperature
Parameters in the diffusivity

Figure 5

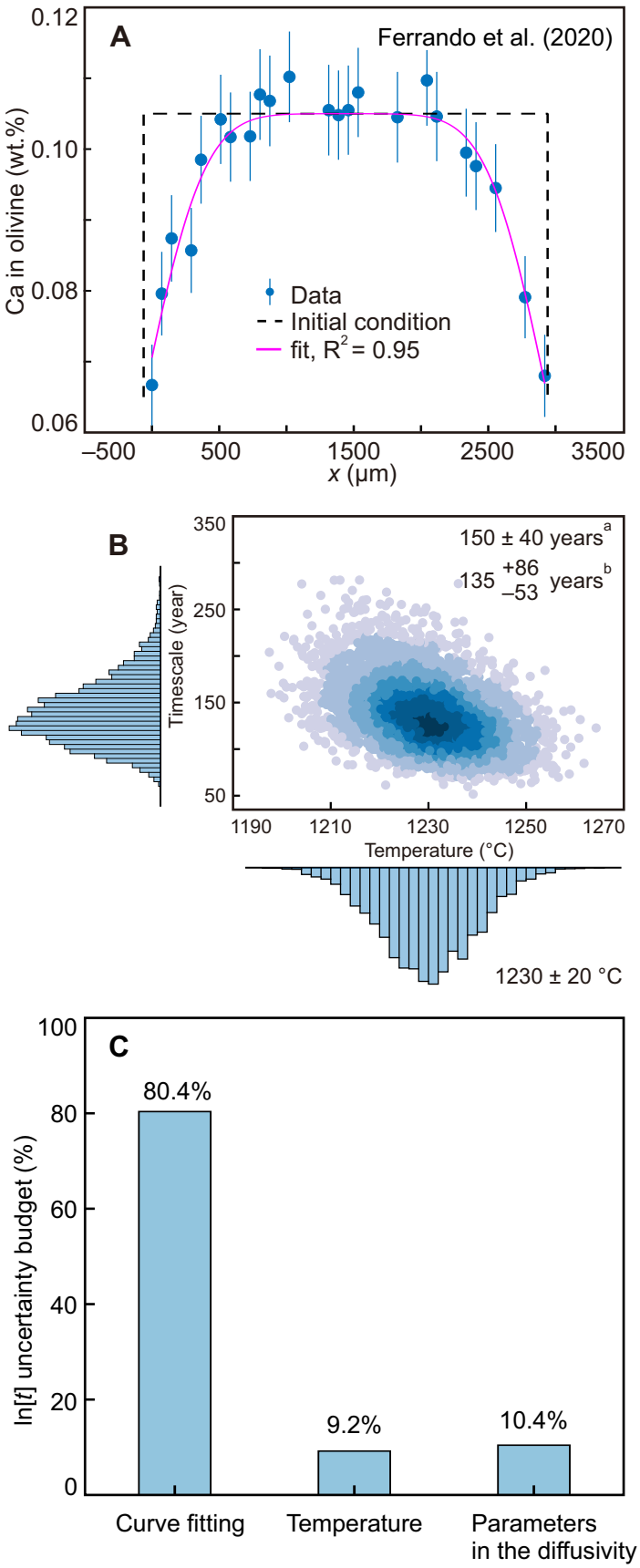
A
Ferrando et al. (2020)
Ca in olivine (wt.%)
0.12
0.10
0.08
0.06
–500
500
1500
2500
3500
x (μm)
Data
Initial condition
fit, R2 = 0.95
B
150 ± 40 years a
135 +86 –53 years b
Timescale (year)
350
250
150
50
1190
1210
1230
1250
1270
Temperature (°C)
1230 ± 20 °C
C
ln[f] uncertainty budget (%)
100
80
60
40
20
0
80.4%
9.2%
10.4%
Curve fitting
Temperature
Parameters in the diffusivity

Figure 6

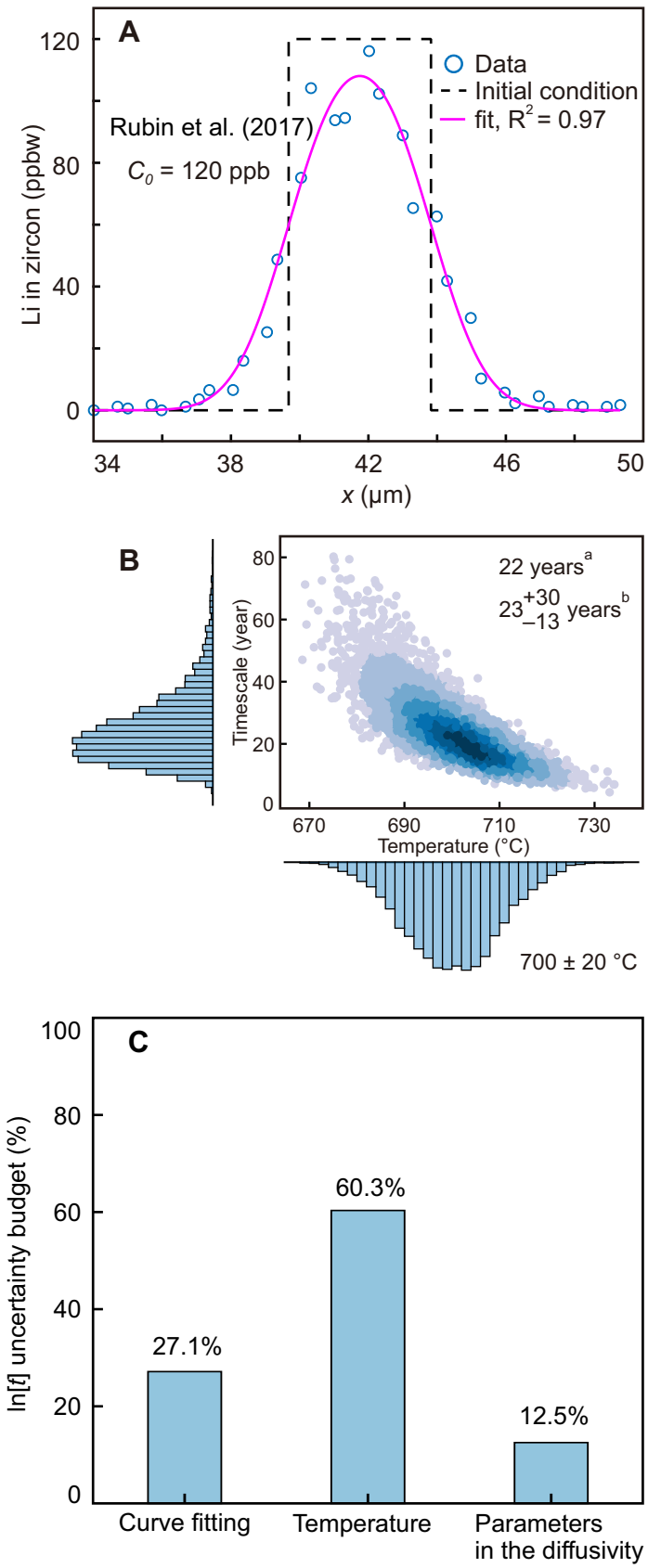
A
Data
Initial condition
fit, R2 = 0.97
Rubin et al. (2017)
C0 = 120 ppb
Li in zircon (ppbw)
x (μm)
B
22 years a
23 +30 −13 years b
Timescale (year)
Temperature (°C)
700 ± 20 °C
C
ln[f] uncertainty budget (%)
27.1%
60.3%
12.5%
Curve fitting
Temperature
Parameters in the diffusivity

Figure 7